

Numerical Modeling of the Effects of Channel Configurations and Inclination Angles Inducing Buoyancy on Reverse Osmosis

N. Zemour^{1†}, A. Azzi¹, O. Rahli¹, A. Al-Sarkhi² and R. L. Gomes³

¹ *University of Sciences and Technology Houari Boumedien (USTHB), FGMGP/LTPMP Bab Ezzouar, Algiers, 16111, Algeria*

² *Department of Mechanical Engineering, King Fahd University of Petroleum & Minerals, Saudi Arabia*

³ *Food Water Waste Research Group, Faculty of Engineering, University of Nottingham, University Park, Nottingham, NG7 2RD, United Kingdom*

†Corresponding Author Email: nacimoil@hotmail.fr

(Received November 3, 2020; accepted January 26, 2021)

ABSTRACT

This numerical study presents a comparison between two different reverse osmosis channel configurations. The physical properties were considered in the computational model as a function of the solute mass fraction. A critical comparison was performed between double-sided membrane channel and single-sided one considering the concentration and flow distribution. Gravitational effect was implemented by introducing the inclination of double membrane geometry for the first time in the literature of reverse osmosis systems. FORTRAN in-house code was developed to resolve conservation equations (mass, momentum, and solute mass fraction) based on the finite volume method. The results of the simulation show that the water recovery factor of double-membrane arrangement is two times higher than the single membrane arrangement. Concentration polarization (CP) can be reduced by both increasing the feed Reynolds number (Re) and decreasing the Aspect Ratio (AR). Considering the cases of low flow rates (up to $Re = 40$) with the flow orientation in the direction of gravity inducing buoyancy effects. The influence of the inclination showed that the average permeate flux, and the water recovery are proportional to the inclination angle up to the maximum values at the right angle (vertical plane).

Keywords: Desalination; Reverse osmosis; Porous membrane; Inclination; CFD; SIMPLE algorithm.

NOMENCLATURE

| | | | |
|------------|--|-----------|--|
| D_{AB} | diffusion coefficient of salt in water | - | |
| H | height of feed channel | u | mean flow velocity at the entrance of the feed channel |
| k | Constant based only on the permeation flux of pure solvent | v | velocity component in y-direction |
| L | length of membrane | Y | recovery factor |
| l | characteristic length-scale in the Grashof number | Y_A | average water recovery factor |
| m_A | salt mass fraction | Q_p | permeation flow rate |
| m_{Aw} | salt mass fraction in the feed side of the membrane | Q_0 | inlet flow rate |
| m_{Ap} | permeation salt mass fraction | J | permeate flow |
| m_{A0} | mass fraction of the salt applied at the inlet | \bar{J} | average permeate flux |
| Δp | pressure difference across the membrane | INC | inclination |
| R | rejection coefficient | MAE | Mean Absolute Error |
| Re | Reynolds number ($Re = 2 \bar{u} H \rho / \mu$) | RMSD | Root Mean Square Deviation |
| | | SWM | Spiral Wound Membrane |
| | | NF | Nanofiltration |
| | | RO | Reverse Osmosis |
| | | α | angle of inclination ° |

| | | | |
|----|--|-------------|---|
| AR | Aspect Ratio | π | osmotic pressure of the solution |
| Sc | Schmidt number ($Sc = \mu / \rho D$) | $\Delta\pi$ | osmotic pressure differential across the membrane |
| u | velocity component in x-direction | μ | viscosity |
| | | ρ | density |

1. INTRODUCTION

Reverse Osmosis (RO) is a membrane separation mechanism, which is considered as the most dominant technology that is used to produce drinking water by desalination (Nicolaisen 2002). The importance of RO is due to its better treatment at relatively reasonable capital and operating costs (Henri 2008) and Menningmann 2018), this aspect has affected the industrial production of desalinated water positively and therefore, it has grown by about 15% per year since 2007 according to Elimelech and Phillip (2011). Various factors such as industrialization and rapid population growth will increase global water demand inducing scarcity. Nowadays, many solutions can be explored to meet the growing needs of fresh water including water desalination by reverse osmosis, which becomes inescapable because of its particularity of being sustainable and low cost solution (Elimelech and Phillip 2011).

A review of seawater desalination mechanism progress and the role of advanced materials in reducing seawater desalination costs were discussed thoroughly by Elimelech and Phillip (2011) and Tata (2009). A steady-state laminar flow was studied for small-scale reverse osmosis system applied to seawater (Abdel-Rahman 2006), which represents a supplementary source for mineral recovery (Jensen *et al.* 2016). Membrane performance enhancement, drop in energy consumption, enhancements in pretreatment processes and plant capacity have been developed for RO desalination over the last decades (UNESCO 2008). Nevertheless, the relatively low water recovery factor (~40%–60%) is among the restrictions of RO (Jensen *et al.* 2016), even if it can be advantageous in avoiding concentration rise beyond the saturation limit (El-Dessouky and Ettouney 2002).

Many papers studied membrane separation processes (Damak *et al.* 2004, Pak *et al.* 2008, de Lima Cunha *et al.* 2014, Marcos *et al.* 2009, Hansen *et al.* 1998, Chen *et al.* 2004, Chen *et al.* 1997, Wang *et al.* 2017 and Huang and Morrissey 1999). Flow in a laboratory membrane filtration cell operated at low recoveries giving a relation between shear stress and velocity may be used when dealing with shear-sensitive suspensions (Tarabara and Wiesner 2003). Hydrodynamics and mass transfer have been examined previously in the empty slight channels and the narrow spacer-filled ones that incorporate obstacles separating the two membranes (Schwinge *et al.* (2002a) PartI, Schwinge *et al.* (2002b) PartII, Schwinge *et al.* (2002c), Amokrane *et al.* (2015a), Amokrane *et al.* (2015b) and Khan 1986). For more comprehension of the physical domain choices in pressure-driven membrane processes applied for RO,

explicit schemes showing a thin flow channel between flat parallel plates (membranes) have been given in a conceptually unwrapped spiral wound reverse osmosis element (Dickson *et al.* 1992 and Li and Tung 2008a). A spiral wound membrane (SWM) sandwich (end-view) clarifies a realistic shape in two dimensions (Chatterjee and Belfort 1986). The fundamental components of a SWM are well illustrated by Schwinge *et al.* (2004).

A very small height typifies the slit-type rectangular channel where saline water flows between two parallel membranes. Such a tight arrangement lowers stream rates to laminar flow resulting in an important concentration polarization issues (Gerlades *et al.* 2001). After predicting flow and mass transfer in an empty nanofiltration (NF) channel that represents a slit-type geometry considered as the basic model of industrial spiral-wound membrane modules (Gerlades *et al.* 2001). Flow has been studied by Gerlades *et al.* (2002a) in narrow rectangular channels with ladder-type spacers to get an insight into laminar regime applied in NF/RO SWM. The inter-spacer regions should ensure a fully developed of both momentum and high concentration profiles (Gerlades *et al.* 2002b, Focke 1983 and Da Costa *et al.* 1994). The effect of the different parameters on the performance of spiral wound reverse osmosis membrane was also described in various works (Madiredi *et al.* (1999), Li *et al.* (2002), Li and Tung (2008b), Radu *et al.* 2010, Karabelas *et al.* 2017, Karabelas 2014 and Karabelas *et al.* 2015). Wardeh and Morvan (2008) in their investigation have analyzed the effect of pressure loss in spacer-filled channels on wall shear stress and salt mass fraction, with the aim of improving the accuracy of the calculations at high pressure. A membrane permeability should be varied with the operating pressure (Alexiadis *et al.* 2007). The intrinsic rejection coefficient is among the most crucial membrane characteristics that have been considered in several works (de Pinho *et al.* 2002 and Amokrane *et al.* 2013). A detailed analysis emphasized the interplay between solute shape and rejection in porous membranes (Vinther *et al.* 2012). The higher the rejection coefficient, the more the occurrence of the fouling phenomenon, sometimes it's a result of a transition between concentration polarization and cake formation which is a severe problem in pressure-driven membrane processes (Chen *et al.* 1997 and Chen *et al.* 2004). During reverse osmosis separation, solutes within the feed flux are convectively driven to the membrane surface where they accumulate and tend to constitute a cake or gel layer. This particle build-up near the membrane surface is called concentration polarization (Lyster and Cohen 2007, Ahmad *et al.* 2005 and Lee and Clark 1998). It is generally admitted that concentration polarization of a solute at the

membrane surface can induce solute adsorption (Cherkasov *et al.* 1995, Nikolova and Islam 1998 and Jönsson 1995), solute precipitation (Jönsson and Jönsson 1996), and gel layer formation (Sablani *et al.* 2001, Khulbe *et al.* 2000, Konieczny and Bodzek 1996 and Denisov 1994). Concentration polarization causes less solvent permeation across the membrane (Miranda and Campos 2001), it can be used also for mass transfer coefficient calculation (Murthy and Gupta 1997). CP is considered to be reversible and can be controlled in a membrane module by means of velocity regulation and other techniques (Sablani *et al.* 2001). Song and Ma (2005) found that spacers with an appropriate geometry may alleviate concentration polarization and increase permeate flux more effectively in spiral wound membrane modules.

The effects of gravity on RO, known also by buoyancy effects have been initiated previously by Fletcher and Wiley (2004) noting the insensitivity of horizontal single membrane channels to gravity. Fletcher and Wiley (2004) findings are in contradiction with those of Youm *et al.* (1996). The latter obtained a significant impact of gravity on horizontal membranes applied for ultrafiltration. The presented literature survey revealed that the difference between single-sided membrane channels and double-sided ones has not been sufficiently undertaken especially for the water recovery quantifying desalination performance knowing that double membrane configurations are closer to industrial membrane setups. It's worth noting that water recovery is a key parameter in choosing industrial RO modules. The present numerical investigation presents a comparison between two types of RO channels according to their setups with the study of the effects of both operating and structural parameters (Re , AR) on double-sided membrane channel performance. An in-house computer code was developed using visual FORTRAN version 6.1 based on Finite Volume Method to predict the mass and the hydrodynamics of the RO in the narrow membrane channels applied to brackish water with a concentration of 2 [g/l] i.e. a salt mass fraction of 0.002 [kg/kg]. Furthermore, the buoyancy effects in double membrane channels according to various inclination angles have been investigated in order to analyze their impact on desalination by RO, which is also considered as the novelty of the present work.

2. MODELING AND GOVERNING EQUATIONS

2.1 Modeling

The problem under consideration is a Reverse Osmosis membrane separation mechanism, induced by flow in a feed channel of length L and height H where the inlet flow is initiated by Poiseuille flow. The case of single-sided membrane channel is shown in Fig. 1 (a). This configuration is already studied numerically by Wardeh and Morvan (2008) and by Fletcher and Wiley (2004), and analyzed in the experimental work proposed by Alexiadis *et al.* (2007). This part will be used only to test the

membrane model validity and to estimate the performances of our numerical code.

The membrane parameters and operating conditions for the single-sided membrane channel, are the same as those proposed in the literature. These parameters are summarized in Tables 1 and 2, respectively used in references (Wardeh and Morvan 2008 and Fletcher and Wiley 2004) and that of the experimental study of Alexiadis *et al.* (2007).

The model extension was carried out according to horizontal double-sided membrane channel arrangement to get closer from feed channel configurations of commercial modules focusing on membrane system disposition (this investigation does not consider spacers presence) (Schwinge *et al.* 2004 and Alexiadis *et al.* 2007).

The aim is to study an empty channel of SWM representing a slit-type setup that constitutes the basic model to be characterized. This basic model is considered the fundamental one and from which more complex models can be derived (Geraldès *et al.* 2001). Several studies described the double membrane disposition, and the feed channels of NF/RO spiral-wound modules, which are always assuming flat surface with parallel semi-permeable membrane walls separated by narrow gaps (Geraldès *et al.* 2000).

The membrane parameters and operational conditions of the extended setup were the same as those used in the previous model represented in Table 1, except the mean flow velocity giving Reynolds number $Re = 100$ (Wardeh and Morvan 2008). Channel dimensions were changed according to the setup proposed by Wardeh and Morvan (2008) (See Table 3).

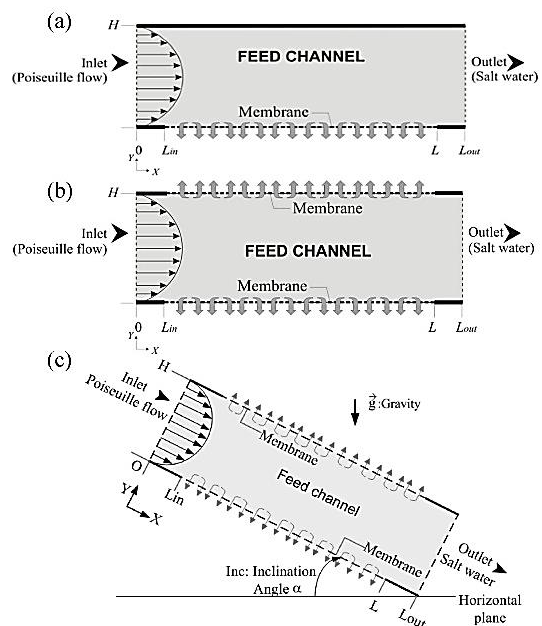


Fig. 1. (a) Horizontal single-sided membrane channel geometry, (b) Horizontal double-sided membrane channel geometry, and (c) Double membrane inclined channel.

Table 1 Model data used for validation with numerical results (Wardah and Morvan 2008 and Fletcher and Wiley 2004).

| | | |
|------------|---|----------------------|
| H | 2 (mm) | Channel dimensions |
| L | 270 (mm) | |
| L_{in} | 20 (mm) | |
| L_{out} | 280 (mm) | |
| m_{A0} | 0.002 (kg kg ⁻¹) | Operating conditions |
| ΔP | 5 x 10 ⁵ (Pa) | |
| \bar{u} | 0.002 (m s ⁻¹) | |
| Re | 8 | |
| R | 0.95 | Membrane parameters |
| k | 2 x 10 ⁻¹⁰ (m s ⁻¹ Pa ⁻¹) | |

Table 2 Model data used for validation with experimental results of Alexiadis *et al.* (2007).

| | | |
|------------|---|----------------------|
| H | 2.5 (mm) | Channel dimensions |
| L | 268 (mm) | |
| L_{in} | 8 (mm) | |
| L_{out} | 276 (mm) | |
| m_{A0} | 0.002 (kg kg ⁻¹) | Operating conditions |
| ΔP | 9 - 14 x 10 ⁵ (Pa) | |
| \bar{u} | 0.03 - 0.3 (m s ⁻¹) | |
| Re | 168 - 1680 | |
| R | 0.95 | Membrane parameters |
| k | 6.93 - 9.72 x 10 ⁻¹² (m s ⁻¹ Pa ⁻¹) | |

Table 3 Model data of the extended model shown in Fig. 1(b)

| | | |
|------------|---|----------------------|
| H | 2 (mm) | Channel dimensions |
| L | 61.5 (mm) | |
| L_{in} | 12 (mm) | |
| L_{out} | 86.5 (mm) | |
| m_{A0} | 0.002 (kg kg ⁻¹) | Operating conditions |
| ΔP | 5 x 10 ⁵ (Pa) | |
| \bar{u} | 0.022 (m s ⁻¹) | |
| Re | 100 | |
| R | 0.95 | Membrane parameters |
| k | 2 x 10 ⁻¹⁰ (m s ⁻¹ Pa ⁻¹) | |

After comparing the two membrane dispositions using the Reynolds number of Table 3. Reynolds number was varied from 100 to 800 in the parametrical study.

Finally, the inclination effect oriented in the gravity direction has been analyzed by considering a double membrane channel as presented in Fig. 1(c). All the parameters data of Table 3 are used, except for Reynolds number and mean flow velocity that changes according to Table 4.

It should be noted that for all configurations, additional regions are added at the inlet L_{in} and exit L_{out} to make sure of a precise execution of the inlet and outlet boundary conditions.

2.2 Governing equations

Two-dimensional steady state equations governing the conservation of mass, x and y momentum and solute mass fraction are presented, respectively as follows:

Continuity:

$$\frac{\partial \rho u}{\partial x} + \frac{\partial \rho v}{\partial y} = 0 \quad (1)$$

Momentum:

x-direction

$$\begin{aligned} \frac{\partial \rho u^2}{\partial x} + \frac{\partial \rho v u}{\partial y} = & -\frac{\partial p}{\partial x} + 2 \frac{\partial}{\partial x} \left(\mu \frac{\partial u}{\partial x} \right) + \\ & \frac{\partial}{\partial y} \left(\mu \left(\frac{\partial u}{\partial y} + \frac{\partial v}{\partial x} \right) \right) - \frac{2}{3} \frac{\partial}{\partial x} \left(\mu \left(\frac{\partial u}{\partial x} + \frac{\partial v}{\partial y} \right) \right) \\ & - \rho g_x \end{aligned} \quad (2)$$

y-direction

$$\begin{aligned} \frac{\partial \rho u v}{\partial x} + \frac{\partial \rho v^2}{\partial y} = & -\frac{\partial p}{\partial y} + 2 \frac{\partial}{\partial y} \left(\mu \frac{\partial v}{\partial y} \right) + \\ & \frac{\partial}{\partial x} \left(\mu \left(\frac{\partial u}{\partial y} + \frac{\partial v}{\partial x} \right) \right) - \frac{2}{3} \frac{\partial}{\partial y} \left(\mu \left(\frac{\partial u}{\partial x} + \frac{\partial v}{\partial y} \right) \right) \\ & - \rho g_y \end{aligned} \quad (3)$$

Solute mass fraction:

$$\begin{aligned} \frac{\partial \rho u m_A}{\partial x} + \frac{\partial \rho v m_A}{\partial y} = & \frac{\partial}{\partial x} \left(\rho D_{AB} \frac{\partial m_A}{\partial x} \right) + \\ & + \frac{\partial}{\partial y} \left(\rho D_{AB} \frac{\partial m_A}{\partial y} \right) \end{aligned} \quad (4)$$

By analogy to Navier-Stokes equations used to investigate the peristaltic transport of a couple stress fluid in a two-dimensional inclined channel according to Mareppa and Sridhar (2015), the body force per unit volume applied in the inclined membrane channel corresponding to the extended model of the present study was written as follows:

x-direction:

$$\rho g_x = -\rho g (\sin \alpha) \quad (5)$$

y-direction:

$$\rho g_y = \rho g (\cos \alpha) \quad (6)$$

A weakly compressible formulation was applied to the flow, as the density depends only on the salt mass fraction (Fletcher and Wiley 2004).

To model the real behavior of RO process with more accuracy, the physical properties of the solution such as viscosity, diffusivity, density, and osmotic pressure vary depending on the solute mass fraction giving mass and flow profiles. Their expressions

involve empirical correlations, which are developed for the first time by Sourirajan (1970), and used after that mainly in the remarkable work of Gerlades *et al.* (2001). Correlations for the variation of physical properties for a salt solution are given by:

$$\pi = 805.1 \times 10^5 m_A [Pa] \quad (7)$$

$$\mu = 0.89 \times 10^{-3} (1 + 1.63 m_A) [Pa.s] \quad (8)$$

$$D_{AB} = \max \left[1.61 \times 10^{-9} (1 - 14 m_A), 1.45 \times 10^{-9} \right] [m^2.s^{-1}] \quad (9)$$

$$\rho = 997.1 + 694 m_A [kg.m^{-3}] \quad (10)$$

These are valid for salt mass fractions up to 0.09

$$[kg.kg^{-1}] \text{ (Gerlades *et al.* (2001)).}$$

2.3 Boundary conditions

The velocity through the membrane is determined by Darcy's law. The pressure is set at the exit channel to zero (since only pressure differences appear in the equations). Hence, a loss of accuracy due to rounding off was avoided (Fletcher and Wiley 2004 and Patankar 1980). The transmembrane velocity is calculated using the following expression:

$$v_w = k(\Delta p - \Delta \pi) \quad (11)$$

where Δp is difference in the pressure across the membrane and $\Delta \pi$ is the differential osmotic pressure across the membrane. k is a constant based only on the permeation flux of pure solvent.

Gauge pressure is set at the exit channel as:

$$p = 0 \quad (12)$$

The following boundary conditions for the velocity components and species are imposed for velocities and solute mass fraction equations.

At the inlet, the fully developed Poiseuille flow is considered and the salt mass fraction is imposed:

$$u = 6u \frac{y}{H} \left(1 - \frac{y}{H} \right) \quad (13)$$

$$v = 0$$

$$m_A = m_{A0}$$

At the impermeable walls, the no-slip condition and no solute flux situation are applied:

$$u = 0$$

$$v = 0 \quad (14)$$

$$\frac{\partial m_A}{\partial y} = 0$$

On the porous membrane, the tangential velocity is set to 0. The permeation velocity, v_w , is formulated.

The diffusive and convective fluxes must balance for the mass fraction of the solute considering the rejection coefficient R that characterizes the membrane selectivity, giving:

$$u = 0$$

$$v = v_w = k(\Delta p - \Delta \pi) \quad (15)$$

$$\rho_w D_{AB} \frac{\partial m_A}{\partial y} + \rho_w m_{Aw} v_w R = 0$$

3. NUMERICAL PROCEDURE

Eqs. (1)-(4) are discretized using a control volume approach with a power-law scheme in approximating the advection terms. SIMPLE algorithm is used to handle coupling between the momentum and continuity equations (Versteeg and Malalasekera 1995 and Popa 2002). All simulations are performed using visual FORTRAN language; there is consequently an essential additional numerical originality.

Given its mixed character, the way the porous membrane boundary condition is treated has a significant influence on the convergence process.

This program develops an iterative line-by-line resolution. Thus, the obtained algebraic system after discretization is solved by combining the TDMA direct method (Tri-Diagonal Matrix Algorithmic) to the iterative Gauss-seidel procedure, with alternating directions resolution. This combined resolution method will allow the information contained at the border to be instantly transmitted to the internal nodes of the domain, unlike the case of a purely iterative method. The salient feature of the current study is the variation of the physical properties in terms of the solute mass fraction (Gerald *et al.* 2001). The convergence of the different correlations that vary for each iteration has been reached.

To ensure convergence of the solution procedure, the relative dependent variables errors are adopted as criteria over the solution domain. The expression is written as follows:

$$\frac{|\phi_{ij}^m - \phi_{ij}^{m-1}|}{|\phi_{ij}^m|} \leq 10^{-5} \quad (16)$$

where ϕ represents a dependent variable, i.e. U, V, m_A, P , the subscripts i, j indicates a grid point and the superscript, m the current iteration.

A non-uniform grid generation of 50 control volumes in the horizontal direction and 20 control volumes in the vertical direction with mesh refining near the porous membrane interface was needed to achieve accurate results from the solving domain according to the grid dependency test. The challenge was to apply an optimal grid that can detect the polarization layer with high precision giving less computational time. Hence, this objective was achieved.

4. RESULTS AND DISCUSSION

For the single and double-sided membranes, the velocity and salt mass fraction profiles across the channel were plotted at the exit plane (Wardeh and Morvan 2008 and Fletcher and Wiley 2004), where the flow is fully established. The comparison is made between two channels with the same dimensions, operational conditions, and membrane parameters. The only difference is the membrane arrangement.

Before including the inclination effects (buoyancy) on the model, the gravity has not been considered because it's oriented normal to the flow direction (Fletcher and Wiley 2004).

The data for the different parameters are indicated in the modeling section.

4.1 Grid Generation

The grid dependency test of the computational domain was carried out initially for a uniform grid along x and y-axes. It was proved that, when the resolution was increased above 50x30, there was a negligible effect on the solution of the transverse velocity. To enhance the computational quality, a non-uniform grid was used by refining the mesh along the y-axis near the porous membrane interface due to the existence of a high concentration profile at this side. Figure 2(a) shows, a non-uniform grid of 50 nodes along the x-axis and 20 nodes along the y-axis resulted in an independent solution, which did not change by improving the resolution, hence less computational time was obtained. Under this refined grid, different values of the adjacent node to the membrane were analyzed. Its optimal position was situated at 5μm from the membrane surface as shown in Fig. 2(b). Therefore, the simulations of the present study were undertaken for a nonuniform grid 50 x 20 including an adjacent node at 5μm from the membrane that represents the optimal mesh.

4.2 Model validation

The validation of our in-house CFD Code is established by comparing our results with those of Wardeh and Morvan (2008) and Fletcher and Wiley (2004) based on numerical procedure. In addition, the model was tested by implementing the same dimensions, membrane parameters, and operational conditions as the experimental work proposed by Alexiadis *et al.* (2007). The fact that this model takes into consideration most of the factors affecting concentration polarization gave to this study more credibility and efficiency (Wardeh and Morvan 2008). This is very crucial for the precision of the operating and modeling of membrane systems.

Figure 3 shows an excellent agreement between the present work and the references Wardeh and Morvan (2008) and Fletcher and Wiley (2004), providing enough confidence in present simulations.

According to the graphs represented in Fig. 4, our code data are verified to be as good as the experimental ones of Alexiadis *et al.* (2007). Thus, our computational model is well validated. The

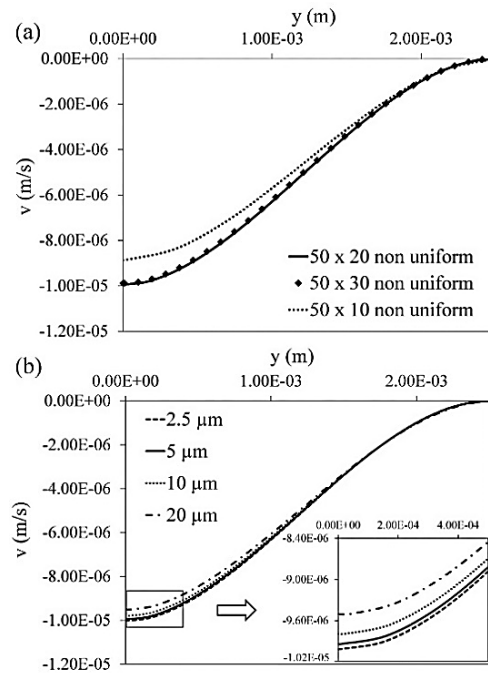


Fig. 2. Transverse velocity variation for (a) various non-uniform grid sizes along y and (b) different dn (distances of the near-wall node to the porous membrane).

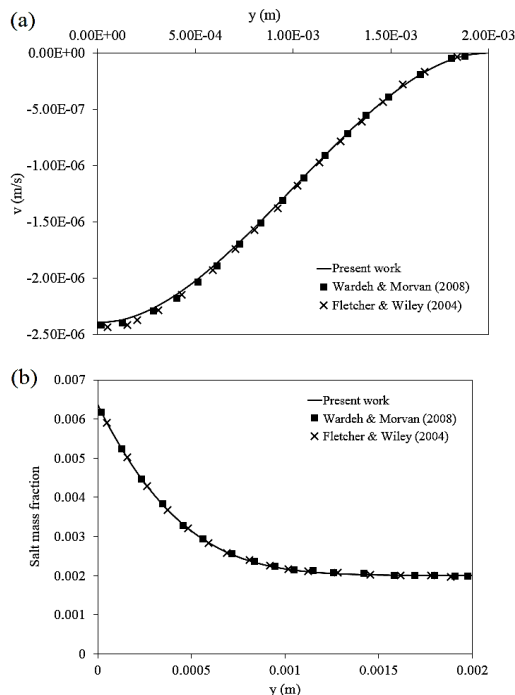


Fig. 3. Numerical results validation: (a) Transverse velocity profile; (b) Transversal salt mass fraction profile.

permeate flow was determined using the conditions reported in Table 2.

The comparison between experimental J_{exp} and numerical J_{num} permeate flow results shown in Fig. 4 was determined for two membrane sets. In the experiment undertaken by [Alexiadis *et al.* \(2007\)](#) the membrane was cut into several samples and could be divided into two categories depending on the permeability values $K_1 = 6.93 \times 10^{-12} [m.s^{-1}.Pa^{-1}]$ and $K_2 = 9.72 \times 10^{-12} [m.s^{-1}.Pa^{-1}]$. The permeate flow as a function of the mean flow velocity was studied for the two cases, low pressure (898.7[kPa]) and high pressure (1398.7[kPa]).

The principal assumption to undertake this validation was the fact that the membrane characteristics remain the same at different pressures. Hence, the compaction effect was neglected giving a constant permeability.

Results represent a good agreement between experiments and computations mainly for K_2 - membrane at high pressure $\Delta P = 1398.7 [kPa]$ giving a Mean Absolute Error (MAE) of 4.48 %. In this case, our results are better than those of [Alexiadis *et al.* \(2007\)](#) having $MAE = 11.28\%$.

At low pressure and for K_2 - membrane, our code performances with $MAE = 8.66\%$ are close to those performed by using CFX4 ([Alexiadis *et al.* \(2007\)](#)).

The values of the mean absolute error MAE and the percentage of root mean square deviation RMSD corresponding to K_1 - membrane are respectively, 8.28% and 11.3%. The choice of the two proposed errors MAE and RMSD is motivated by the fact that they are the most commonly used criteria for evaluating errors in many published papers in the literature like [Slimani *et al.* \(2017\)](#) and many more and consequently expected to be more reliable.

The Percentage of the Root Mean Square Deviation (RMSD) and the Absolute Mean Percentage Error (MAE) are shown in Eq. (17) and (18) ([Slimani *et al.* \(2017\)](#)).

$$MAE(\%) = \frac{100}{n} \sum_1^n \left| \frac{X_{sim,i} - X_{exp,i}}{X_{exp,i}} \right| \quad (17)$$

$$MSD(\%) = 100 \times \sqrt{\frac{\sum_1^n \left(\frac{X_{sim,i} - X_{exp,i}}{X_{sim,i}} \right)^2}{n}} \quad (18)$$

where $X_{sim,i}$, $X_{exp,i}$ and n represent the simulated values, the experimental values, and the data number, respectively.

4.3 Influence of channel configurations

Figure 5(a) shows the variation of the transverse velocity, v , with distance y for single and double sided membrane. For a single-sided membrane channel, the transverse velocity is maximum with a minus sign at the porous membrane then it decreases with y until it reaches zero at the non-membrane

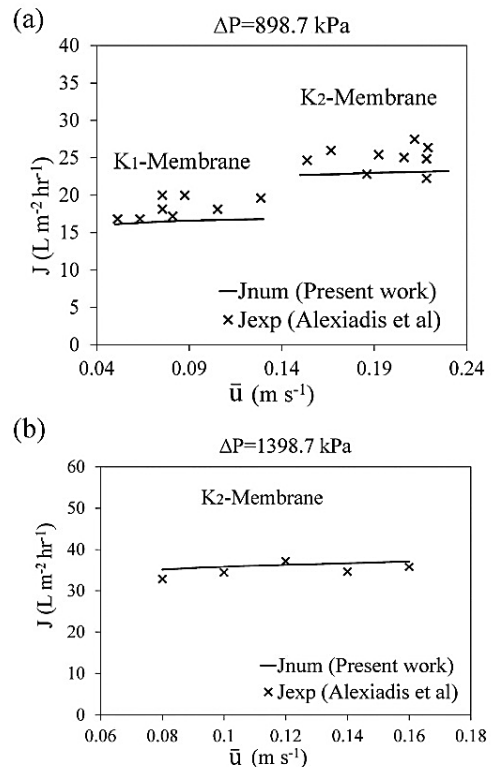


Fig. 4. Comparison between present work J_{num} and experimental study J_{exp} for different cross-flow velocities at (a) low transmembrane pressures including K_1 and K_2 - membranes and (b) high transmembrane pressures for K_2 - membrane.

wall. As for the the double membrane channel there are two maximum values for the transverse velocity with different signs depending on the y -axis.

To give a physical meaning to the velocity, the absolute value should be used knowing that the sign inquires us about the flow direction as a function of y -axis orientation.

Figure 5(b) shows the increase of the mass fraction of the solute near the porous membranes that is due to the polarization layer formation for both single and double-membrane configurations. m_{Aw} obtained at the feed side of the membrane surfaces is three times as high as m_{AO} applied at the channel inlets resulting in the same values at channels middles with

$$0.002 [kg.kg^{-1}],$$

which is in agreement with the previous works of [Wardah and Morvan \(2008\)](#) and [Fletcher and Wiley \(2004\)](#) applying the same transmembrane pressures under laminar flow conditions. The difference between the two arrangements is that the other side of the single membrane channel represents a non-membrane wall without permeation and consequently, no polarization layer build-up, where the solute mass fraction value joints the inlet one with

$$0.002 [kg.kg^{-1}].$$

According to Baker (2004), Wardeh (2008) and by analogy with Geraldès *et al.* (2002) The recovery factor is calculated by the relation shown in Eq.(19):

$$Y = \frac{Q_p}{Q_0} \quad (19)$$

Figure 5(c) shows that the water recovery profile indicating the membrane performance is two times bigger in the case of double-sided membrane channel $Y_A=3.05\%$ because of its feed flow decomposition into two transversal components acting on the two membranes resulting in more permeation in addition to the axial flux (brine) at the channel outlet. Thus, the profile behavior seems to be similar but the one with the double-sided membrane geometry gives 200% of one side membrane channel efficiency in matters of water recovery ($Y_A=1.52\%$ for one side membrane channel).

Knowing that:

$$Y_A = \frac{1}{L - L_{in}} \int_{L_{in}}^L Y(x).dx \quad (20)$$

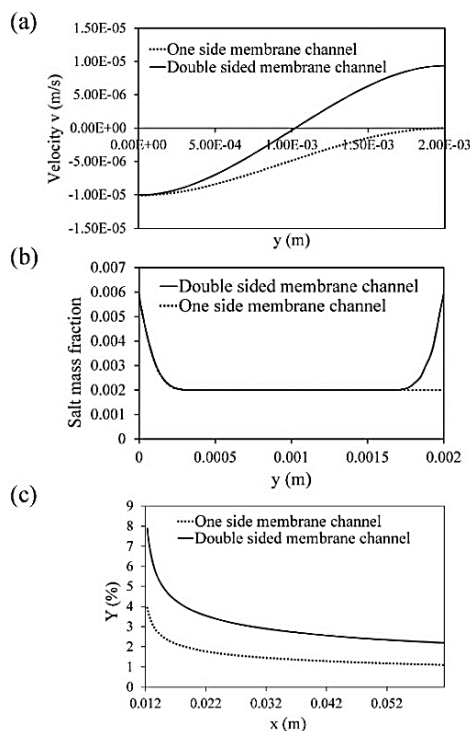


Fig. 5. Comparison of (a) transverse velocity profiles at exit plane, (b) transversal distributions of salt mass fraction at exit plane and (c) water recovery along the porous membrane.

In the following sections, the influence of Reynolds number, Re , (which represents the ratio of inertial to viscous forces), the aspect ratio, AR , (defined by the height of the channel reported to its total length) and gravity (highlighted as a function of the inclination of the channel) will be presented for the case of the two-sided membrane channel. It is worth to mention

here that the flow is inclined downward (i.e. the gravity is contributing in the main flow direction).

4.3 Effect of Reynolds number

It can be seen in Fig. 6(a) that the axial velocity was fully developed at the inlet and took the Poiseuille profile. The axial velocity increases with Reynolds number which is obvious from the relation between Re and axial velocity that are linked by the mean flow velocity term at the channel entrance as

$$Re = \frac{2\bar{u}H\rho}{\mu} \quad \text{and} \quad u = 6\bar{u}\frac{y}{H}\left(1 - \frac{y}{H}\right) \quad \text{have a}$$

proportional relationship with, \bar{u} .

Figure 6(b) shows a proportional relationship between the transverse velocity and Reynolds number. It is affected by the inlet velocity enhancement that elevates all the hydrodynamics components (one axial and two transversals in the porous membranes directions). It has to be noted that the transverse velocity is equal to zero in the middle of the channel $y=0.001$ [m] due to the pure axial flow at that location.

According to Fig. 6(c), the permeate flux increases along the membrane with the Reynolds number enhancement, but the average water recovery in the channel lowers from 3.05 % for $Re = 100$ to 0.66 % for $Re = 800$ (A fall of 78 %). Hence, when Reynolds number rises, it gives an amount of the mean flow velocity constituting the denominator of water recovery factor more prominent than the amount of resulting permeate velocity (Permeate velocity represents the numerator of water recovery factor).

The results of Fig. 6(d) are considered as a logical support to interpret the findings of Fig. 6(c). The osmotic pressure depending on solute mass fraction equals 1.61×10^5 [Pa] for $m_{A0} = 0.002$ [kg.kg⁻¹].

At the membrane outlet, the solute mass fraction near the porous membrane was not significantly impacted by Reynolds number rise, about ~ 10% of concentration change (decrease) resulting in a large effect on the permeate flux increase ~ 85%. This is due to the osmotic pressure, which is very close to the pressure difference applied across the membrane. Therefore, the effective pressure generating the dynamics, that is very low, becomes very sensitive to the concentration change and results in an apparent permeate flux variation. Figure 6(d) Shows that the more the Reynolds number increases from 100 to 800, the less the polarization layer takes place. The shear effects induced by Re rise impedes the salt convection towards the porous membrane, and consequently constrains the concentration boundary layer growth. These results confirm the concentration profiles already obtained by Damak *et al.* (2004) for ultrafiltration and the mass boundary layer decrease according to Reynolds number enhancement in microfiltration noted by Pak *et al.* (2008). Schmidt number used in these two studies Damak *et al.* (2004) and Pak *et al.* (2008) is equal to 1000 while Schmidt number of ~ 572, which is typical of Sodium Chloride according to Schwinge *et al.*

(2002c) has been used in the present paper. $Sc = \frac{\mu}{\rho D}$ according to Pak *et al.* (2008) and Miranda and Campos (2001). Both Sc number values are in nonfiltration ranges of interests (Gerald *et al.* 2002) $570 < Sc < 3200$. The permeate flux is improved due to the salt accumulation decrease when raising Re representing less resistance against the permeation.

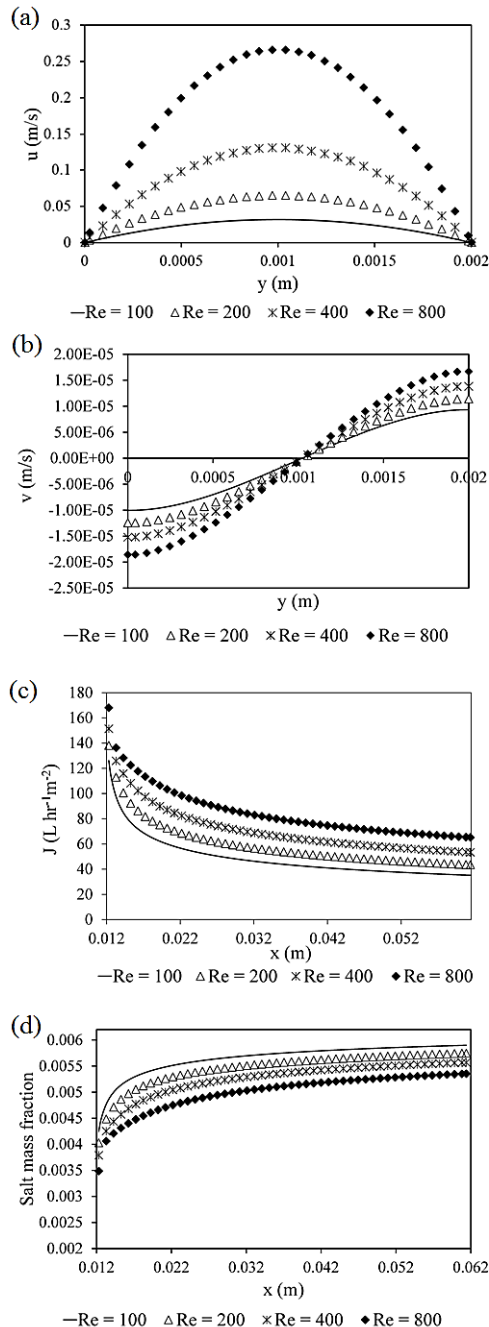


Fig. 6. Reynolds number effect on (a) the axial velocity, (b) the transverse velocity, (c) the permeate flux along the membrane and (d) the solute mass fraction distribution along the membrane.

4.4 Effect of Aspect Ratio

The total length of the channel is maintained constant, and its height is changed to vary the Aspect Ratio. The Aspect Ratio taken as a reference was $AR = 0.023$, that represents the extended model (see Table 3). The channel height is multiplied by two and then divided by two to analyze the impact of its variation on desalination.

Figure 7(a) shows that the higher the Aspect Ratio, the lower the permeate flux at the porous membrane. The permeate flow at the membrane inlet is 3 to 5 times higher than the membrane exit for both AR values. It's practically the same order of magnitude obtained previously by Wardeh and Morvan (2008) and by Fletcher and Wiley (2004) for the extraction velocity along the membrane having the same shape as the permeate flow. This depends on salt accumulation on the membrane surface as shown in Fig. 7(b). The AR and the permeate flux are in inverse proportion. If the aspect ratio is reduced to one-fourth (1/4) of $AR = 0.048$ to get $AR = 0.012$, the average water recovery gain is 485 % in the channel.

Solutes are convectively pushed to the perm-selective membrane at which they accumulate. The particles build-up near the membrane surface constitute the polarization layer as it's shown in Fig. 7(b) which relatively slows down the water permeation through the pores. The Aspect Ratio rise enhances the concentration polarization and reduces the solvent extraction as it's shown in Fig. 7(a). Therefore, the AR and the concentration polarization are in a direct proportional relationship.

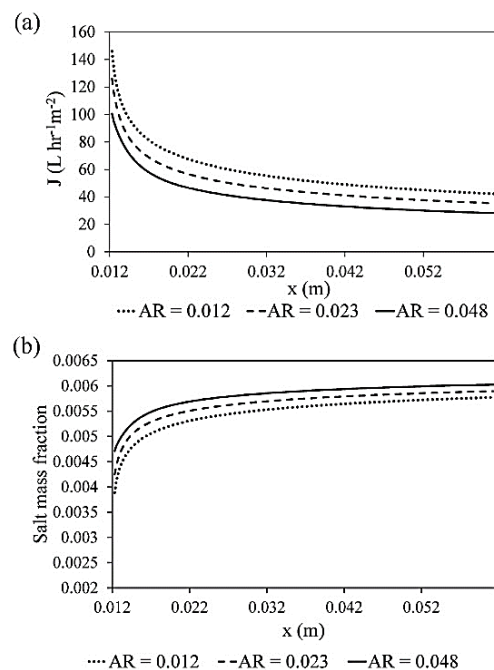


Fig. 7. Aspect Ratio effect on (a) permeate flux and (b) salt fraction distribution along the membrane.

4.4 Impact of channel inclination

Fletcher and Wiley (2004) have concluded that reverse osmosis in horizontal single membrane channels are insensitive to the gravity and consequently the buoyancy effects are neglected for horizontal channel cases. The originality of our case came from the fact that the simulations were performed for double-sided membrane arrangement taking into account channel inclination in the direction of gravity, which has never been studied before in the literature of reverse osmosis systems.

Simulation results were not available for the lowest inlet velocity $\bar{u} = 0.002 [m.s^{-1}]$. Hence, water recovery factor was not applicable because of calculation bugs.

In fact the mean flow velocity $\bar{u} = 0.002 [m.s^{-1}]$ representing the axial velocity at the channel inlet corresponds to $Re = 8$. In the case of double-sided membrane arrangement and under this low regime the flow cannot act in three directions (one axial in the direction of the channel exit and two transversal in the direction of the two membranes). This is contrary to the single sided membrane channel used by Fletcher and Wiley (2004) where the flow pushed just in two directions. Hence, the lowest applicable Reynolds number for which buoyancy effect can appear must be greater than $Re = 8$ in the case of the inclined double-membrane channel with the gravity component performing in the direction of the flow.

The inclination rise improved water recovery and obtained its maximum for the lowest applicable Reynolds number of $Re = 20$ as seen in Table 4. For $Re = 20$, the average percentage of the water recovery increase (gain) of the vertical case (90°) compared to the horizontal case is about 5.86% and for the 60° case compared to horizontal is about 5.09% (also gain).

As for the laminar high flow rate cases ($Re > 20$), water recovery factor variation as a function of inclination angle is very small and insignificant. No variation in water recovery has been noticed for $Re = 400$. Table 5 shows that the average permeate flux is proportional to the inclination angle for $Re = 20$. The more the inclination is close to the vertical axis the more the permeate flux is recuperated and vice versa. A significant rise of 1.3 and 1.5 $[L.m^{-2}.h^{-1}]$ respectively were obtained for inclinations of 45° and 60° when compared with the horizontal case. Interestingly, Fig. 8(a) shows that the average salt mass fraction along the membrane does not decrease significantly (about $\sim 0.3 - 0.5\%$) with changing the inclination. Nevertheless, the average permeate flux is highly impacted by this small variation of the high concentration profile (it's enhanced by $\sim 5 - 6\%$) according to Fig. 8(b). This behavior is due to the sensitivity of permeate flux to the effective pressure. The applied differential pressure and the differential osmotic pressure values are close to

each other mainly at the channel outlet resulting a remarkably low effective pressure that is highly sensitive to the solute mass fraction. Thus, inclination rise produces more permeate flow across the membrane and reaches the maximum at the vertical case as it can be seen in Fig. 8(b). This is a consequence of the drop in salt accumulation along the membrane which is diminishing the resistance against water permeation as seen in Fig. 8(a). Permeate flux is closer to its maximum value corresponding to the vertical channel for an inclination angle of 60° . Gravitational effects arise due to the difference in density between the solution of the feed and the concentration polarization at the permselective membrane. Considering the free and forced convection, the effects of buoyancy are governed by the division of the Grashof number and the Reynolds number squared (Fletcher and Wiley 2004), i.e.

$$Gr/Re^2 = (g.\Delta\rho.l^3.\rho / \mu^2) / (2.\bar{u}.H.\rho / \mu)^2 = g.\Delta\rho.l^3 / 4.H^2.\rho.u.^2$$

Accordingly, it's obvious that gravitational effects are anticipated to be more important when the gravity acts along the inclined $l \sim L.\sin \alpha$ and vertical ($l=L$) channels rather than normal to it for the horizontal one ($l=H$, or more precisely $l= \delta$, where δ is the solute boundary layer thickness). In the horizontal case, the normal boundary layer thickness is very small. It means that the hydrostatic pressure generated by buoyancy is negligible. Hence, there is independency between the horizontal channel and buoyancy effects.

The fluid extraction generates the difference in the density, $\Delta\rho$, shown in the equation shown above.

Table 4 Average water recovery factor $Y_A(\%)$ for different inlet velocities and channel inclinations. The gravity is acting with the flow of the double membrane channel (NA) Not Applicable.

| $\bar{u} [m.s^{-1}]$ | 0.002 | 0.005 | 0.009 | 0.022 | 0.088 |
|----------------------|-------|-------|-------|-------|-------|
| Re | 8 | 20 | 40 | 100 | 400 |
| Inc 0° | NA | 7.85 | 5.55 | 3.05 | 1.05 |
| Inc 30° | NA | 8.09 | 5.61 | 3.06 | 1.05 |
| Inc 45° | NA | 8.19 | 5.64 | 3.07 | 1.05 |
| Inc 60° | NA | 8.25 | 5.66 | 3.07 | 1.05 |
| Inc 90° | NA | 8.31 | 5.67 | 3.07 | 1.05 |

Table 5 Average permeate flux \bar{J} depending on inclination angles for low flow rate $Re = 20$.

| Inclination | $\bar{J} [L.m^{-2}.h^{-1}]$ |
|----------------------|-----------------------------|
| Horizontal 0° | 28.5 |
| Inc 30° | 29.4 |
| Inc 45° | 29.8 |
| Inc 60° | 30 |
| Vertical 90° | 30.2 |

$$\bar{J} = \frac{1}{L - L_{in}} \int_{L_{in}}^L J(x) dx$$

5. CONCLUSION

An in-house FORTRAN code based on the finite volume method has been developed and validated to investigate numerically the RO desalination applied for brackish water in narrow membrane channels. The results showed that water recovery factor in double-membrane configuration is two times bigger than single membrane channel. In the case of the horizontal double-membrane channel, salt mass fraction distribution along the membrane is directly proportional to the Aspect Ratio and inversely proportional to Reynolds number. A remarkable Reynolds number impact on permeate flux and water recovery results was obtained. Increasing Reynolds number from 100 to 800, resulted in enhancement of permeate flux accompanied with water recovery losses of 78% of its value. Concerning the Aspect Ratio influence, Reducing the AR to one-fourth (1/4) of AR = 0.048, resulted in a large gain in the average water recovery of about 485%.

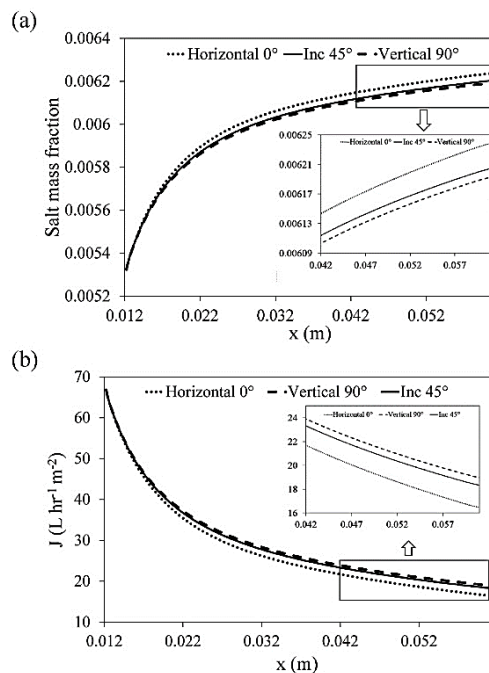


Fig. 8. Inclination impact on (a) salt mass fraction accumulation along the membrane and (b) permeate flux for Re = 20 corresponding to the highest buoyancy sensitivity.

The variation of the inclination angle was undertaken considering downward flow orientation i.e. in the gravity direction. The increase in inclination substantially induced buoyancy phenomenon only for low flow rates that has Re less than 40 excluding Re = 8. For high laminar flow (Re > 40), no noteworthy buoyancy effects have been noticed. Hence, water recovery and permeation flux become insensitive to the inclination angle. For Re = 20,

corresponding to the highest membrane performance, the inclination effects were important. The more the angle of inclination is (from horizontal) the more the water recovery is enhanced. The average water recovery factor gain was about 5.09 % for 60° and 5.86% (as a maximum) for 90° compared to the horizontal channel case. In general, inclination promotes permeation and reduces concentration polarization along the porous membrane for low flow rates.

REFERENCES

- Abdel-Rahman, A. K. (2006). Numerical modeling of reverse osmosis desalination systems. *The 2nd International Conference on Water Resources and Arid Environment*.
- Ahmad, A. L., K. K. Lau, M. Z. Abu Bakar and S. R. Abd. Shukor (2005). Integrated CFD simulation of concentration polarization in narrow membrane channel. *Computers & Chemical Engineering* 29, 2087–2095.
- Alexiadis, A., D. E. Wiley, A. Vishnoi, R. H. K. Lee, D.F. Fletcher and J. Bao (2007). CFD modelling of reverse osmosis membrane flow and validation with experimental results. *Desalination* 217, 242-250.
- Amokrane, M., D. Sadaoui and M. Dudeck (2013). Modélisation thermodynamique et simulation numérique du procédé de purification d'une solution aqueuse par Osmose Inverse. *21^{ème} Congrès Français de Mécanique*, Bordeaux.
- Amokrane, M., D. Sadaoui, C. P. Koutsou, A. J. Karabelas and M. Dudeck (2015a). A study of flow field and concentration polarization evolution in membrane channels with two-dimensional spacers during water desalination. *Journal of Membrane Science* 477, 139-150.
- Amokrane, M., D. Sadaoui, M. Dudeck and C. P. Koutsou (2015b). New spacer designs for the performance improvement of the zigzag spacer configuration in spiral-wound membrane modules. *Desalination and Water Treatment* 57, 5266-5274.
- Baker, R. W. (2004). *Membrane technology and applications*. John Wiley & Sons Ltd.
- Chatterjee, S. G. and G. Belfort (1986). Fluid flow in an idealized spiral wound membrane module. *Journal of Membrane Science* 28, 191-208.
- Chen, J. C., Q. Li and M. Elimelech (2004). In situ monitoring techniques for concentration polarization and fouling phenomena in membrane filtration. *Advances in Colloid and Interface Science* 107, 83-108.
- Chen, V., A. G. Fane, S. Madaeni and I. G. Wenten (1997). Particle deposition during membrane filtration of colloids: transition between concentration polarization and cake formation. *Journal of Membrane Science* 125, 109-122.
- Cherkasov, A. N., S. V. Tsareva and A. E. Polotsky

- (1995). Selective properties of ultrafiltration membranes from the standpoint of concentration polarization and adsorption phenomena. *Journal of Membrane Science* 104, 157-164.
- Da Costa, A. R., A. G. Fane and D. E. Wiley (1994). Spacer characterization and pressure drop modelling in spacer-filled channels for ultrafiltration. *Journal of Membrane Science* 87, 79-98.
- Damak, K, A. Ayadi, P. Schmitz and B. Zeghmati (2004). Modeling of crossflow membrane separation processes under laminar flow conditions in tubular membrane. *Desalination* 168, 231-239.
- de Lima Cunha, A., J. S. de Souza, S. R. de Farias Neto, A. G. B. de Lima and E. S. Barbose (2014). Separation Process by Porous Membranes, A Numerical Investigation. *Advances in Mechanical Engineering* 6, 1-9.
- de Pinho, M. N., V. Semião and V. Geraldes (2002). Integrated modeling of transport processes in fluid/nanofiltration membrane systems. *Journal of Membrane Science* 206, 189-200.
- Denisov, G. A. (1994). Theory of concentration polarization in cross-flow ultrafiltration gel layer model and osmotic-pressure model. *Journal of Membrane Science* 91, 173-187.
- Dickson, J. M., J. Spencer and M. L. Costa (1992). Dilute. single and mixed solute systems in a spiral wound reverse osmosis module Part I: Theoretical model development. *Desalination* 89, 63-88.
- El-Dessouky, H. T. and H. M. Ettouney (2002). *Fundamentals of Salt Water Desalination*. Department of Chemical Engineering, College of Engineering and Petroleum, Kuwait University, Kuwait.
- Elimelech, M. and W. A. Phillip (2011). The future of seawater desalination, Energy, Technology and the Environment. *Science* 333, 712-717.
- Fletcher, D. F. and D. E. Wiley (2004). A computational fluids dynamics study of buoyancy effects in reverse osmosis. *Journal of Membrane Science* 245, 175-181.
- Focke, W. W. (1983). On the mechanism of transfer enhancement by eddy promoters. *Electrochim. Acta* 28, 1137-1146.
- Geraldes, V. M., V. A. Semiao and M. N. de Pinho (2002a). Flow management in nanofiltration spiral wound modules with ladder-type spacers. *Journal of Membrane Science* 203, 87-102.
- Geraldes, V., V. Semião and M. N. de Pinho (2001). Flow and mass transfer modelling of nanofiltration. *Journal of Membrane Science* 191, 109-128.
- Geraldes, V., V. Semiao and M. N. de Pinho (2002b). The effect on mass transfer of momentum and concentration boundary layers at the entrance region of a slit with a nanofiltration membrane wall. *Chemical Engineering Science* 57 735 – 748.
- Geraldes, V, V. Semião and M. N. Pinho (2000). Numerical modelling of mass transfer in slits with semi-permeable membrane walls. *Engineering Computations* 17, 192-218.
- Hansen, M., V. A. Baker and O. Hassager (1998). Spectral element simulation of ultrafiltration. *Chemical Engineering Science* · 53, 3099-3115.
- Henri, B. (2008). *General council for the environment and sustainable development water, energy, desalination and climate change in Mediterranean*, blue Plan, Sophia Antipolis, France.
- Huang, L. and M. T. Morrissey (1999). Finite element analysis as a tool for crossflow membrane filter simulation. *Journal of Membrane Science* 155, 19-30.
- Jensen, C. A. Q., E. Drioli and F. Macedonio (2016). Integrated Membrane Desalination Systems with Membrane Crystallization Units for Resource Recovery: A New Approach for Mining from the Sea. *Crystals* 6, 1-13.
- Jönsson, A. S. (1995). Concentration polarization and fouling during ultrafiltration of colloidal suspensions and hydrophobic solutes. *Separation Science and Technology* 30, 301-312.
- Jönsson, A. S. and B. Jönsson (1996). Colloidal fouling during ultrafiltration. *Sep. Sci. Technol.* 31, 2611-2620.
- Karabelas, A. J. (2014). Key issues for improving the design and operation of membrane modules for desalination plants. *Desalination and Water Treatment* 52, 1820-1832.
- Karabelas, A. J., M. Kostoglou and C. P. Koutsou (2015). Modeling of spiral wound membrane desalination modules and plants - Review and research priorities. *Desalination* 356, 165–186.
- Karabelas, J., C. P. Koutsou and D. C. Sioutopoulos (2017). Comprehensive performance assessment of spacers in spiral-wound membrane modules accounting for compressibility effects. *Journal of Membrane Science* 549, 602-615.
- Khan, A. H. (1986). *Desalination Processes and Multistage Flash Distillation Practice*. Elsevier Science Publishers, New York.
- Khulbe, K. C., T. Matsuura, S. Singh, G. Lamarche, S. H. Noh (2000). Study on fouling of ultrafiltration membrane by electron spin resonance. *Journal of Membrane Science* 167, 263-273.
- Konieczny, K. and M. Bodzek (1996). Ultrafiltration of latex wastewaters. *Desalination* 104, 75-82.
- Lee, Y. and M. M. Clark (1998). Modeling of flux decline during crossflow ultrafiltration of

- colloidal suspensions. *Journal of Membrane Science* 149, 181-202.
- Li, F., W. Meindersma, A. B. Haan, T. Reith (2002). Optimization of commercial net spacers in spiral wound membrane modules. *Journal of Membrane Science* 208, 289–302.
- Li, Y. and K. Tung (2008a). CFD simulation of fluid flow through spacer-filled membrane module: selecting suitable cell types for periodic boundary conditions. *Desalination* 233, 351-358.
- Li, Y. and K. Tung (2008b). The effect of curvature of a spacer-filled channel on fluid flow in spiral-wound membrane modules. *Journal of Membrane Science* 319, 286-297.
- Lyster, E. and Y. Cohen (2007). Numerical study of concentration polarization in a rectangular reverse osmosis membrane channel: Permeate flux variation and hydrodynamic end effects. *Journal of Membrane Science* 303, 140–153.
- Madireddi, K., B. Babcock, B. Levine, J. H. Kim and M. K. Stenstrom (1999). An unsteady-state model to predict concentration polarization in commercial spiral wound membranes. *Journal of Membrane Science* 157, 13-34.
- Marcos, B., C. Moresoli, J. Skorepova and B. Vaughan (2009). CFD modeling of a transient hollow fiber ultrafiltration system for protein concentration. *Journal of Membrane Science* 337, 136–144.
- Mareppa, M. and N. G. Sridhar (2015). Peristaltic Transport of a Couple Stress Fluid with Slip Effects in an Inclined Channel. I. J. A. P. R. R. *International Peer Reviewed Refereed Journal* 2, 01-11.
- Miranda, J. M. and J. B. L. M. Campos (2001). Concentration polarization in a membrane placed under an impinging jet confined by a conical wall — a numerical approach. *Journal of Membrane Science* 182, 257–270.
- Murthy, Z. V. P. and S. K. Gupta (1997). Estimation of mass transfer coefficient using a combined nonlinear membrane transport and film theory model. *Desalination* 109, 39-49.
- Nicolaisen, B. (2002). Developments in membrane technology for water treatment. *Desalination* 153, 355-360.
- Nikolova, J. D. and M. A. Islam (1998). Contribution of adsorbed layer resistance to the flux-decline in an ultrafiltration process. *Journal of Membrane Science* 146, 105-111.
- Pak, A., T. Mohammadi, S. M. Hosseinalipour, and V. Allahdini (2008). CFD modeling of porous membranes. *Desalination* 222, 482-488.
- Patankar, S. V. (1980). *Numerical Heat Transfer and Fluid Flow*. New York, McGraw-Hill.
- Popa, L. C. (2002). *Numerical modelling of heat transfer by the finite volume method*, Craiova University, Roumania.
- Radu, A. I., J. S. Vrouwenvelder, M. C. M. van Loosdrecht and C. Picoreanu (2010). Modeling the effect of biofilm formation on reverse osmosis performance: Flux, feed channel pressure drop and solute passage. *Journal of Membrane Science* 365, 1-15.
- Sablani, S. S., M. F. A. Goosen, R. Al-Belushi, M. Wilf (2001). Concentration polarization in ultrafiltration and reverse osmosis: a critical review. *Desalination* 141, 269-289.
- Schwinge, J., D. E. Wiley and D. F. Fletcher (2002a). Simulation of Flow Around Spacer Filaments Between Channel Walls. Part I: Hydrodynamics. *Industrial & Engineering Chemistry Research* 41, 2977–2987.
- Schwinge, J., D. E. Wiley and D. F. Fletcher (2002b). A CFD Study of Unsteady Flow in Narrow Spacer-filled Channels for Spiral Wound Membrane Modules. *Desalination* 146, 195-201.
- Schwinge, J., D. E. Wiley and D. F. Fletcher (2002c). Simulation of Flow Around Spacer Filaments Between Channel Walls. Part II: Mass Transfer. *Industrial & Engineering Chemistry Research* 41, 4879–4888.
- Schwinge, J., P. R. Neal, D. E. Wiley, D. F. Fletcher and A. G. Fane (2004). Spiral wound modules and spacers, Review and analysis. *Journal of Membrane Science* 242, 129-153.
- Slimani, M. A., M. Amirat, I. Kurucz, S. Bahria, A. Hamidat, W. B. Chaouch (2017). A detailed thermal-electrical model of three photovoltaic/thermal (PV/T) hybrid air collectors and photovoltaic (PV) module: Comparative study under Algiers climatic conditions. *Energy Conversion and Management* 133, 458–476.
- Song, L. and S. Ma (2005). Numerical Studies of the Impact of Spacer Geometry on Concentration Polarization in Spiral Wound Membrane Modules. *Industrial & Engineering Chemistry Research* 44, 7638-7645.
- Sourirajan, S. (1970). *Reverse Osmosis*. Academic Press, New York.
- Tarabara, V. V. and M. R. Wiesner (2003). Computational fluid dynamics modeling of the flow in a laboratory membrane filtration cell operated at low recoveries. *Chemical Engineering Science* 58, 239–246.
- Tata, F. (2009). Sea water desalination : Assessment of the latest technological advances, economic assessment, critical analysis depending on the context. Institut for life and environmental sciences and industries, Paris.
- UNESCO (2008). Emerging Trends in Desalination: A Review. Centre for Membrane Science and Technology University of New South Wales, National Water Commission, Canberra,

- Australia.
- Versteeg, H. K. and W. Malalasekera (1995). *An introduction to computational fluid dynamics: the finite volume method*. Longman Scientific & Technical, New York.
- Vinther, F., M. Pinelo, M. Brøns, G. Jonsson and A. S. Meyer (2012). Statistical modelling of the interplay between solute shape and rejection in porous membranes. *Separation and Purification Technology* 89, 261–269.
- Wang, Y., L. Fortunato, S. Jeong and T. Leiknes (2017). Gravity-driven membrane system for secondary wastewater effluent treatment: Filtration performance and fouling characterization. *Separation and Purification Technology* 184, 26-33.
- Wardeh, S. (2008). *Numerical Modelling of Reverse Osmosis Channels : Application in Desalination Industry*. Dissertation, Univeristy of Nottingham, UK.
- Wardeh, S. and H. P. Morvan (2008). CFD simulations of flow and concentration polarization in spacer-filled channels for application to water desalination. *Chemical Engineering Research and Design* 86, 1107-1116.
- Youm, K. H., A. G. Fane and D. E. Wiley (1996). Effects of natural convection instability on membrane performance in dead-end and cross-flow ultrafiltration. *Journal of Membrane Science* 116: 229-241.